doi:10.1016/j.jmb.2011.02.038 J. Mol. Biol. (2011) 408, 262–276

Contents lists available at www.sciencedirect.com

Journal of Molecular Biology

journal homepage: http://ees.elsevier.com.jmb

Viral RNAi Suppressor Reversibly Binds siRNA to Outcompete Dicer and RISC via Multiple Turnover

Renata A. Rawlings[1,2], Vishalakshi Krishnan[2] and Nils G. Walter[2]*

[1]Biophysics, University of Michigan, 930 North University Avenue, Ann Arbor, MI 48109-1055, USA
[2]Department of Chemistry, University of Michigan, 930 North University Avenue, Ann Arbor, MI 48109-1055, USA

Received 22 May 2010;
received in revised form
2 February 2011;
accepted 16 February 2011
Available online
24 February 2011

Edited by J. Doudna

Keywords:
fluorescence quenching;
p19;
RNA interference;
systems biology modeling;
viral silencing suppressor protein

RNA interference is a conserved gene regulatory mechanism employed by most eukaryotes as a key component of their innate immune response to viruses and retrotransposons. During viral infection, the RNase-III-type endonuclease Dicer cleaves viral double-stranded RNA into small interfering RNAs (siRNAs) 21–24 nucleotides in length and helps load them into the RNA-induced silencing complex (RISC) to guide the cleavage of complementary viral RNA. As a countermeasure, many viruses have evolved viral RNA silencing suppressors (RSS) that tightly, and presumably quantitatively, bind siRNAs to thwart RNA-interference-mediated degradation. Viral RSS proteins also act across kingdoms as potential immunosuppressors in gene therapeutic applications. Here we report fluorescence quenching and electrophoretic mobility shift assays that probe siRNA binding by the dimeric RSS p19 from Carnation Italian Ringspot Virus, as well as by human Dicer and RISC assembly complexes. We find that the siRNA:p19 interaction is readily reversible, characterized by rapid binding [$(1.69 \pm 0.07) \times 10^8$ M^{-1} s^{-1}] and marked dissociation ($k_{off} = 0.062 \pm 0.002$ s^{-1}). We also observe that p19 efficiently competes with recombinant Dicer and inhibits the formation of RISC-related assembly complexes found in human cell extract. Computational modeling based on these results provides evidence for the transient formation of a ternary complex between siRNA, human Dicer, and p19. An expanded model of RNA silencing indicates that multiple turnover by reversible binding of siRNAs potentiates the efficiency of the suppressor protein. Our predictive model is expected to be applicable to the dosing of p19 as a silencing suppressor in viral gene therapy.

Introduction

Over the past decade, RNA interference (RNAi) has become recognized as a benchmark laboratory and potential clinical tool to control gene expression, as well as a highly conserved eukaryotic immune response to viral pathogens or transposons.[1–4] During viral infection, plant and invertebrate cells are known to activate RNAi, where viral RNA is specifically recognized by the cytoplasmic RNase-III-type endonuclease Dicer and degraded by an RNA-induced silencing complex (RISC). Dicer cleaves exposed stretches of double-stranded RNA into small interfering RNAs (siRNAs) 21–24 nucleotides in length

*Corresponding author. E-mail address: nwalter@umich.edu.

Abbreviations used: siRNA, small interfering RNA; RISC, RNA-induced silencing complex; RSS, RNA silencing suppressors; RNAi, RNA interference; CIRV, Carnation Italian Ringspot Virus; EMSA, electrophoretic mobility shift assay; SP, siRNA:p19; SD, siRNA:Dicer; SDP, siRNA:Dicer:p19; T/F, tetramethylrhodamine/fluorescein; FRET, fluorescence resonance energy transfer; miRNA, microRNA; EDTA, ethylenediaminetetraacetic acid.

(depending on species). Dicer then delivers the double-stranded siRNA, via the RISC-loading complex,[5] to RISC,[6,7] where the passenger strand of the duplex is cleaved and released, while the guide strand is retained to guide specific cleavage of complementary viral RNA genomes or transcripts.[8,9] Dicer is thus thought to play a critical dual role in RNAi by both generating virus-specific siRNA duplexes and assembling them with the necessary protein components into active RISC.[10] In mammalian cells, including human cells, artificial siRNAs have been shown to confer antiviral immunity,[11] but only very recently has evidence emerged to suggest that small RNAs, including siRNAs, are also directly generated from infecting viruses.[12]

To subvert the host RNAi response, many viruses have evolved small proteins that act as RNA silencing suppressors (RSS).[13,14] One of the best characterized RSS is exemplified in the plant pathogen Carnation Italian Ringspot Virus (CIRV), which encodes a 19-kDa protein termed p19, an important pathogenicity factor that is highly conserved among all tombusviruses.[14] Crystal structures[15,16] and recent molecular dynamics simulations[17] show that homodimers of p19 bind a single siRNA duplex in a positively charged surface cleft (Fig. 1a). Pairs of tryptophan residues stack on both terminal base pairs to establish a sequence-independent caliper-like size selection for siRNA duplexes with 19 bp and 2-nucleotide-long 3′-overhangs. Sequestration and binding of Dicer-generated siRNAs by p19 have been observed to correlate with reduced viral RNA degradation, systemic symptom spread, and sustainability of viral phenotype after infection.[18–21] Previous electrophoretic mobility shift assays (EMSAs) have suggested that the affinity of dimeric p19 for siRNA is high, with an apparent equilibrium dissociation constant of $K_p = 0.17 \pm 0.02$ nM.[15] Such tight binding is consistent with a widely accepted sequestration model wherein the p19 dimer near-quantitatively binds siRNA duplexes to suppress RNAi.[14,18] Binding of double-stranded RNA is considered to be the most common RSS mechanism,[22,23] yet measurements of siRNA binding and dissociation kinetics to better understand sequestration have not been reported to date for any RSS protein.

Here we develop solution-based fluorescence quenching assays that observe siRNA:p19 (SP) binding to be readily reversible, with not only a rapid

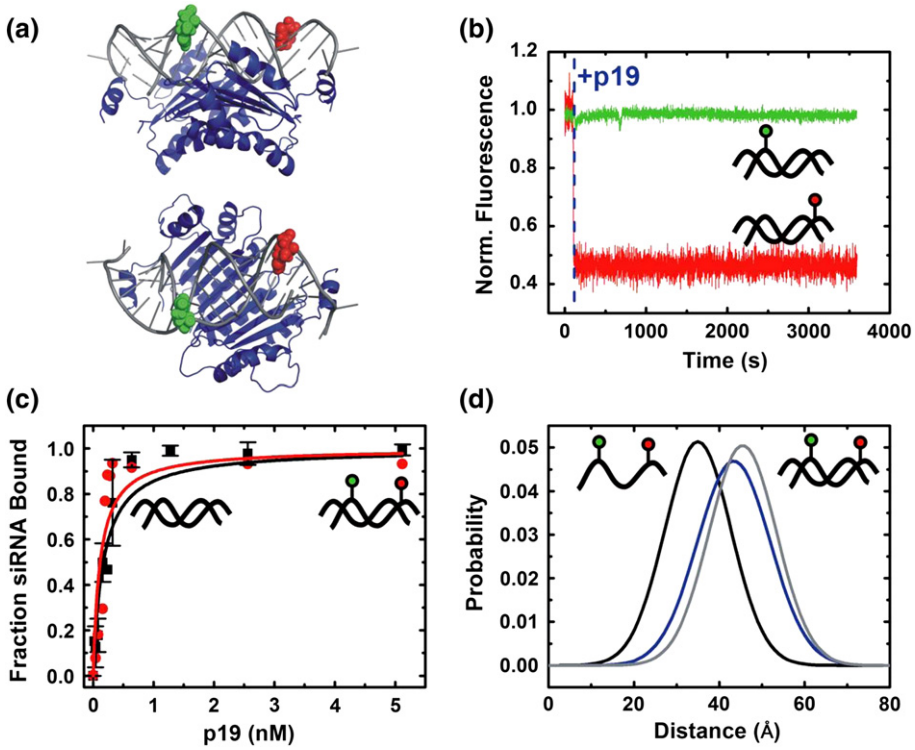

Fig. 1. Fluorescence assays to detect SP complex formation. (a) Crystal structure of p19 (blue) bound to an siRNA (gray). The nucleotides to which the fluorophores fluorescein (F) and tetramethylrhodamine (T) are attached are highlighted in green and red, respectively. (b) The T-only labeled siRNA (red) is quenched upon p19 addition, while the F-only labeled siRNA (green) is unaffected by p19. (c) EMSA analysis shows that the doubly, F and T labeled siRNA (red) binds to p19 with the same affinity as the unlabeled siRNA (black). (d) Time-resolved FRET measures the F-to-T distance distributions with the corresponding mean F-to-T distances for the single-stranded, protein-free double-stranded (black), and p19-bound double-stranded (blue) siRNA (gray) at 35 Å, 43.4 Å, and 44.5 Å, respectively.

binding rate constant [$(1.69 \pm 0.07) \times 10^8$ M^{-1} s^{-1}] but also a dissociation rate constant ($k_{off} = 0.062 \pm 0.002$ s^{-1}) markedly faster than those of slow-release nucleic acid binding proteins.[24,25] Our results are consistent, within error, with the high apparent affinity measured in EMSAs, yet expand on the sequestration model. If binding were completely irreversible, it would require the virus to generate sufficient quantities of p19 dimer to quantitatively bind all small RNAs produced enzymatically by either Dicer cleavage or amplification effected in a plant cell through RNA-dependent RNA polymerase.[2] By contrast, facile reversibility of SP complex formation opens the possibility that multiple turnover may potentiate p19's efficacy as RSS. In particular, if p19 were to disrupt siRNA:Dicer (SD) interaction via multiple turnover, it would potently interfere with the role of Dicer as obligatory RISC assembly factor.

Consistent with such a mechanism of p19 action, we observe the efficient competition of p19 for siRNA binding with active recombinant human Dicer in the absence of other known RISC components, as well as the prominent disruption of RISC assembly complexes observed in human HeLa cell extract containing the three core RISC-loading complex components Dicer, TRBP, and Ago2.[5] Mathematical modeling demonstrates that the Dicer competition data are only accurately reproduced by assuming the formation of a transient ternary complex, siRNA:Dicer:p19 (SDP). Taken together, there emerges a multiple-turnover "catch-and-release" mechanism, wherein p19 repeatedly promotes the dissociation of SD complexes to efficiently suppress Dicer-mediated RISC assembly.

Results

Fluorescence assays to observe SP complex formation

We site-specifically labeled the antisense (guide) strand of an established luciferase-targeting siRNA duplex[26,27] with either fluorescein or tetramethylrhodamine as fluorescence quenching probe in positions not expected to interfere with p19 binding (Fig. 1a). We found that only the tetramethylrhodamine label was efficiently quenched upon p19 addition (Fig. 1b). Addition of buffer or other proteins such as recombinant Dicer caused no such quenching (Fig. S2). To observe a robust quenching signal upon p19 addition, we proceeded to label with

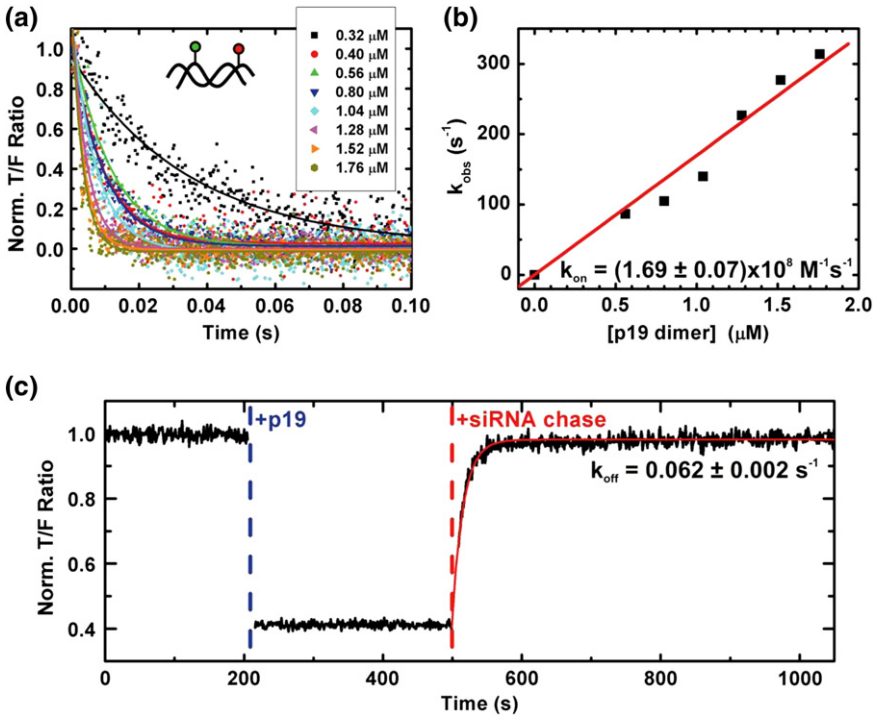

Fig. 2. Kinetics of the formation and dissociation of the SP complex. (a) Pseudo-first-order kinetics of the binding of doubly labeled siRNA (50 nM) to excess p19, measured through the T/F ratio during stopped-flow mixing. Scatter points denote raw data; lines denote single-exponential fits to extract rate constants. (b) Plot of the observed pseudo-first-rate constants from (a) over the p19 concentration. The linear fit yields the indicated bimolecular binding rate constant k_{on}. (c) Fluorescence detection of the binding of doubly labeled siRNA (50 nM) to p19 (500 nM) and of complex dissociation upon addition of an unlabeled siRNA chase (3 μM). A single-exponential fit (red line) yields the indicated dissociation rate constant k_{off}.

both fluorophores together, allowing us to monitor a normalized tetramethylrhodamine/fluorescein (T/F) fluorescence ratio that is insensitive to dilution effects and other perturbations of an otherwise relative fluorescence signal. Next, we tested by EMSA the p19 binding of this doubly labeled siRNA against that of the unlabeled siRNA and detected no interference from the fluorophores ($K_p = 0.17 \pm 0.03$ nM in both cases), consistent with earlier EMSA studies[15] (Fig. 1c). Time-resolved fluorescence resonance energy transfer (FRET) between the two fluorophores revealed only a small increase in fluorophore distance distribution upon p19 addition (with the mean distance increasing from 43.4 Å to 44.5 Å; Fig. 1d), indicating that formation of the SP complex leads to only a minor deformation of the siRNA duplex, as expected from X-ray crystallography.[15] We conclude that the doubly labeled siRNA duplex is a suitable reporter for the formation of the SP interaction in solution.

p19 binds siRNA rapidly and reversibly

Addition of increasing excess concentrations of p19 to the doubly labeled siRNA led to an increase in the pseudo-first-order rate constant of tetramethylrhodamine quenching, as monitored by the T/F ratio, yielding a bimolecular binding rate constant of $k_{on} = (1.69 \pm 0.07) \times 10^8$ M^{-1} s^{-1} (Fig. 2a and b). Next, dissociation of the preformed SP complex was monitored upon the addition of a large excess of unlabeled siRNA (chase), yielding a dissociation rate constant of $k_{off} = 0.062 \pm 0.002$ s^{-1} (Fig. 2c; Fig. S2). Together with rapid k_{on}, a solution-based dissociation equilibrium constant of $k_{off}/k_{on} = K_{p,sol} = 0.37 \pm 0.08$ nM is obtained within 2-fold of the EMSA-predicted value (0.17 nM), attesting to a high-affinity yet also notably reversible SP binding mode.

p19 efficiently competes with recombinant human Dicer for siRNA binding

The critical dual role of Dicer in RNAi as the enzyme that produces siRNAs and as an RISC assembly factor[10] suggests the SD interaction as a particularly vulnerable step during RNA silencing. Previous studies in embryo extracts of the fruit fly *Drosophila* have shown that p19 suppresses RNA silencing by competing with the Dcr2–R2D2 complex.[18,22] To determine whether p19 also competes with human Dicer for siRNA, we employed EMSA using radiolabeled siRNA duplexes and an active recombinant human Dicer preparation devoid of other known RISC proteins (Fig. S1) [available as a relatively crude purification of heterologously overexpressed Dicer (Genlantis); see Materials and Methods]. We measured the apparent equilibrium dissociation constant of the human SD complex as $K_d = 3.7 \pm 0.4$ nM (Fig. 3a; Fig. S3a). The presence of a low concentration of p19 (0.17 nM), equivalent to the K_p of the SP complex, weakened this interaction by >25-fold to ~100 nM (Fig. 3a; Fig. S3b). The presence of a saturating concentration of p19 (2.5 nM) weakened the interaction still further by

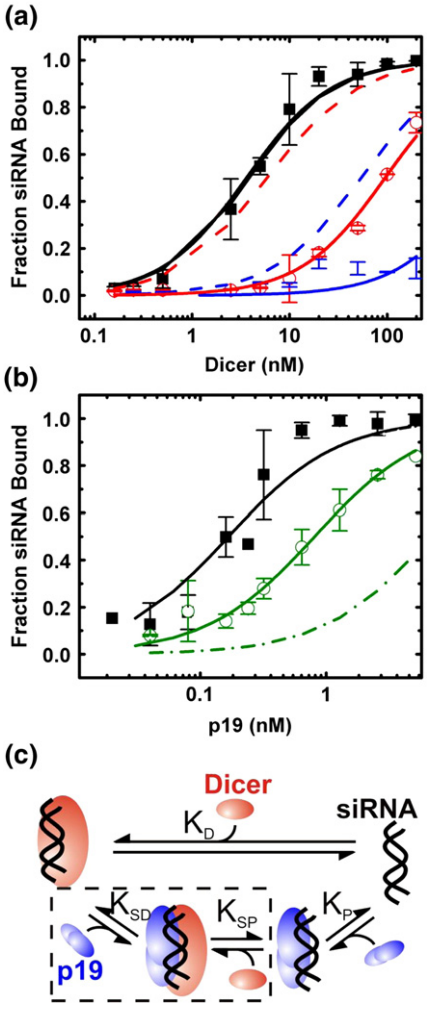

Fig. 3. Competition of p19 with human Dicer for siRNA binding, as detected by EMSA. (a) The fraction of siRNA bound to Dicer over increasing Dicer concentrations in the absence of p19 (black squares) and in the presence of 0.17 nM (open red circles) or 2.5 nM p19 (blue dots). Continuous lines indicate the corresponding fits of hyperbolic binding isotherms. Dashed lines indicate the predicted curves based on a dissociative binding mechanism (siRNA has to first dissociate from Dicer to bind p19). (b) Fraction of siRNA bound to p19 over increasing p19 concentrations in the absence (black squares) or in the presence of a saturating Dicer concentration of 140 nM (open green circles). Continuous lines indicate the corresponding fits of hyperbolic binding isotherms. The dot/dash line indicates the predicted curve based on a dissociative binding mechanism. (c) Schematic of the two competition models between Dicer and p19 for siRNA; the dashed box highlights the part unique to the ternary complex formation model.

>270-fold to an estimated lower limit of ~1.0 μM (Fig. 3a; Fig. S3c). These findings led us to hypothesize that p19 can function to inhibit RNAi in humans by interrupting the SD complex before Dicer can hand off siRNA to RISC. Reciprocal competition experiments showed that the presence of even saturating concentrations (140 nM) of Dicer lowered the apparent affinity of p19 for siRNA only marginally (~4-fold from 0.17 ± 0.03 nM to 0.81 ± 0.06 nM; Fig. 3b; Fig. S3d and e), further supporting the hypothesis that strong competition with the SD complex is an important mode of action for p19 inhibition of RNAi in human cells.

Human siRNA-containing complexes formed in cytosolic cell extract are vulnerable to p19 challenge

Previous studies with *Drosophila* extracts have shown that p19 inhibits RISC assembly while disrupting preassembled RISC to a lesser extent.[22] Our result that p19 disrupts the complex of recombinant human Dicer with siRNA suggests that p19 may also be effective in suppressing RISC assembly in mammals. To test this hypothesis and to probe p19's effect on the formation of human RISC-related complexes, we used a modified *in vitro* RISC assembly assay.[28,29] Specifically, we incubated radiolabeled siRNA duplex with 15% (vol/vol) cytosolic HeLa cell extract, which we showed to contain the three core RISC-loading complex components Dicer, TRBP, and Ago2 (Figs. S1 and S5), and analyzed the products by EMSA and autoradiography (Fig. 4a and b). We observed three distinct siRNA-containing complexes that correspond to those previously observed, including a slowly migrating complex D that is thought to contain Dicer, as well as two faster-migrating bands termed C1 and C2[18,30] (Fig. 4b). The normalized fraction of complex C2 decreases over a 2-h period, whereas the complex C1 and D fractions increase (with estimated rate constants of 2×10^{-3} s^{-1}, 0.8×10^{-3} s^{-1}, and 0.4×10^{-3} s^{-1}, respectively; Fig. 4a). To test for the presence of Dicer, we performed supershift assays with anti-Dicer polyclonal antibody and found that only complex D specifically supershifts with this antibody (Fig. 4c). Similarly, Dicer is detected by Western blot analysis in complex D only (Fig. S5). Notably, adding increasing p19 concentrations to the cell extract prior to siRNA addition increasingly impairs the formation of all three siRNA-containing complexes, concomitant with an accumulation of the competing SP complex (Fig. 4d and e). When p19 is added to the RISC assembly assay after 2 h of preincubation with siRNA, the formation of particularly the Dicer-containing complex D is inhibited to a lesser extent (Fig. 4f and g). Similar results were obtained at higher HeLa cell extract concentrations and temperatures (Fig. S4).

Modeling supports the formation of a transient ternary SDP complex

The mechanism of competition between p19 and human Dicer can be determined from mathematically modeling the two possible modes of competition for a two-protein/single-substrate system. First, competition may occur through dissociative binding mode, where the higher-affinity protein shifts the relative equilibrium of the system by binding all of the available substrate as it dissociates from the competitor, thus establishing a new equilibrium position (Fig. 3c). In the case of p19 and Dicer, siRNAs are preassociated with Dicer at the onset due to their cleavage from longer RNAs, making such dissociative binding by p19 relatively fast only if spontaneous dissociation from Dicer is rapid. Second, competition may occur through formation of a ternary complex intermediate involving siRNA, Dicer, and p19 (Fig. 3c). Using the previously determined gel-based apparent dissociation equilibrium constants for p19 ($K_p = 0.17 \pm 0.02$ nM) and Dicer ($K_d = 3.7 \pm 0.4$ nM), we can discriminate between these two possible modes of competition by calculating the resulting expected SD and SP complex fractions and by comparing them to experiments for a given set of equilibrium conditions.[31]

Assumption of the dissociative binding mechanism shows a poor correlation with experiments, as evident from the fact that changes upon Dicer addition are consistently overestimated (Fig. 3a) while changes upon p19 addition are consistently underestimated (Fig. 3b). This poor correlation suggests that ternary complex formation is needed to explain the observed efficient disruption of the SD complex in the presence of p19. The inclusion of ternary complex formation in the mechanism creates a thermodynamic cycle that requires a K_d/K_{sp} ratio equal to the K_p/K_{sd} ratio.[32] Rearranging and using the values of K_d and K_p, we find that $K_{sp}/K_{sd} = K_d/K_p = 21.6$ and, therefore, $K_{sp} = 21.6K_{sd}$. This result suggests that dissociation of the ternary complex into the binary SP complex is >20-fold more likely than dissociation into the SD complex, indicating that siRNAs can indeed be effectively shuttled toward the p19-bound state by assuming the transient formation of a ternary SDP complex. The resulting model correlates well with experiments and explains both the weak effect that Dicer addition has on the SP complex and the large effect that p19 addition has on the SD complex (Fig. 3a and b). A similar result is observed when p19 is placed in the context of the RNAi pathway, as follows.

Modeling illustrates the benefits of reversible siRNA binding by p19

To further interpret and unify our results, we expanded a previously published, simplified

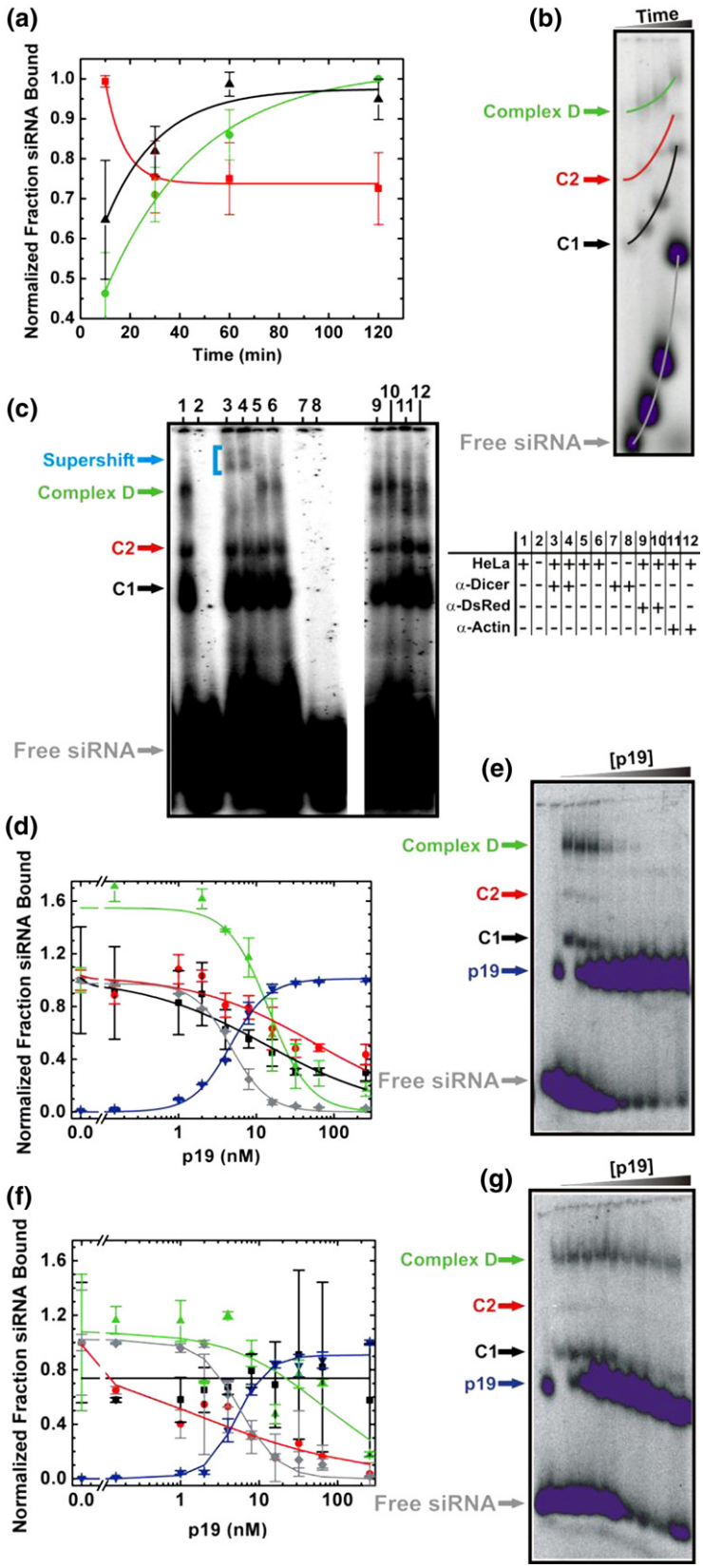

Fig. 4. Competition of p19 with human siRNA-containing complexes found in cytosolic HeLa cell extract. (a) Normalized fraction of siRNA bound to complexes D (green), C2 (red), and C1 (black), where the highest point is normalized to unity in each complex over time, as derived from the gel in (b). The relative abundances of complexes C1 and D increase over time with estimated rate constants of 8×10^{-4} s^{-1} and 4×10^{-4} s^{-1}, respectively, whereas C2 decreases in relative abundance with a rate constant of 2×10^{-3} s^{-1} (all derived from single-exponential fits as indicated). (b) Formation of complexes D, C2, and C1 after 10 min, 30 min, 60 min, and 120 min of incubation of siRNA in cytosolic HeLa cell extract. Samples were loaded onto a running 4% native polyacrylamide gel, leading to the indicated differences in migration. (c) Anti-Dicer antibody-based supershift of siRNA-containing complexes. Dicer containing complex D shifts in the presence of anti-Dicer antibody (lane 3, 0.8 μg; lane 4, 1.6 μg). Lanes 1, 5, and 6 indicate the mobility of the complexes in the absence of any antibody. Lanes 9–12 show negative controls where 0.8 μg or 1.6 μg of anti-actin antibody (lanes 9 and 10) or anti-DsRed antibody (lanes 11 and 12) was added. (d) Quantification of the normalized fraction of siRNA bound in each complex, as derived from gels as in (e). Fractions were normalized to the zero time point and fit with binding isotherms. (e) Formation of complexes after 2.5 h of incubation of siRNA in cytosolic HeLa cell extract and increasing concentrations of p19. (f) Quantification of the normalized fraction of siRNA bound in each complex, as derived from gels as in (e), normalized as in (d) and fit with binding isotherms. (g) Formation of complexes D, C1, and C2 after 2 h of incubation of siRNA in cytosolic HeLa cell extract, followed by the addition of increasing concentrations of p19 and further incubation for 30 min.

steady-state kinetic model that encapsulates key features of the RNAi pathway, including RNA cleavage by Dicer, siRNA incorporation into RISC, and the resulting RISC-mediated RNA degradation.[33] We included the experimentally observed competition of p19 with the SD interaction and p19's reversible interaction with siRNA. From this model, there emerges the possibility of a multiple-turnover "catch-and-release" mechanism wherein p19 is effectively recycled after successfully competing with Dicer and dissociating again from the siRNA (Fig. 5a). We next sought to establish what impact, if any, such a mechanism has on the ability of p19 to suppress RNAi (for details of the model and its analysis, see Supplementary Information).

Our model suggests that the intracellular steady-state load of viral proteins (and thus viral viability) is specified by three global parameters (Fig. 5a): the efficiencies of Dicer (A), RNAi in the specific host cell type (y), and p19 (v). These three global parameters are each composed of detailed mechanistic parameters (Table 1 and Supplementary Information). In the case of the irreversible binding of p19 to an siRNA (single turnover), the relative enhancement of viral protein load in the presence of p19 over the absence of p19, ϕ_{Irr}, is then described by:

$$\phi_{Irr} = \frac{2Av(1+y)}{\left(-1-v+\sqrt{1+2(1+A)v+(-1+A)^2v^2}\right)y + Av(2+y)}$$

(compare Fig. 4e and g), suggesting that, indeed, early stages of viral infection (where n is small) may be most effective for RNAi suppression by p19. The relative enhancement of viral protein load in the presence of p19 over the absence of p19 in our reversible binding model, ϕ_{Rev}, is then described by:

$$\phi_{Rev} = \frac{2Av(1+y)}{2Av + y\left(1 - aA\frac{k_{off}}{k_{cat_D}} + v - Av - \sqrt{\left(-4A\left(-1+a\frac{k_{off}}{k_{cat_D}}(A-n)\right)\frac{v}{\beta^2} + \left(-1+aA\frac{k_{off}}{k_{cat_D}} + (-1+A)v\right)^2\right)}\right)}$$

0.1 and 200. Reversible siRNA binding by p19 is thus found to enhance viral protein production by up to ~2.2-fold over that observed for the irreversible binding model (Fig. 5b). Notably, even a value of $n = 0.1$ does not diminish this effect much due to a close-to-linear decrease in ϕ_{Rev} toward unity, with an increase in n toward unity (data not shown).

Discussion

The small positive-sense single-stranded RNA genome of tombusviruses encodes p19, an RSS thought to be critical for symptom spread and for leading to a negligible dependence on the p19 suppression efficiency v (Fig. 5b) when using a realistic parameter space (Table 1 and Materials and Methods).

In the case of a reversibly formed SP complex, as observed in our experimental work, two additional model parameters come into play (Fig. 5a): the fraction of siRNAs that successfully reenters the RNAi pathway after release from p19 (n) and the fraction of total p19 that is bound to siRNA (a). Values of n close to zero lead to a recycling of p19 protein without a reincorporation of the released siRNA into RISC, whereas values of n close to unity effectively reduce the free concentration of p19 without changing the fate of the bound siRNA as an eventual guide for RISC. Previous studies have shown that Dicer substrates at subnanomolar concentrations are up to 100-fold more effective in gene knockdown than mature siRNAs,[6,37] suggesting a low probability of $n = 0.01$ for reincorporation of free siRNA into the RNAi pathway especially at the low siRNA concentrations expected during the early stages of viral infection. Previous experimental studies in *Drosophila* embryo lysate have shown that p19 is effective in preventing low nanomolar concentrations of siRNAs from incorporating into RISC but is less effective in disrupting mature RISC,[18,22] a feature that is also evident in our data where k_{off} is the dissociation constant of the SP complex, and k_{cat_D} is the cleavage rate constant of Dicer. This model predicts a hyperbolic dependence of ϕ_{Rev} on the p19 efficiency v, with little dependence on a (Fig. 5b), which can be estimated from our experimental data in Fig. 3a and b to range between

the cytotoxicity of this class of plant pathogens[20,21,38,39] through its ability to bind and thus sequester Dicer-generated siRNAs.[14,18] The proposed use of p19 in therapeutic and research applications, including mammalian gene therapy,[40] vaccine production,[41,42] and as human retroviral protein homolog,[43] motivates the study of p19 outside its natural host environment, across kingdom boundaries. We here have investigated the binding of a generic siRNA by CIRV p19 through fluorescence quenching assays in combination with radioactive EMSAs. The noticeable dissociation of an siRNA from p19 ($k_{off} = 0.062 \pm 0.002\ s^{-1}$) is counterbalanced by fast association to yield a solution-based

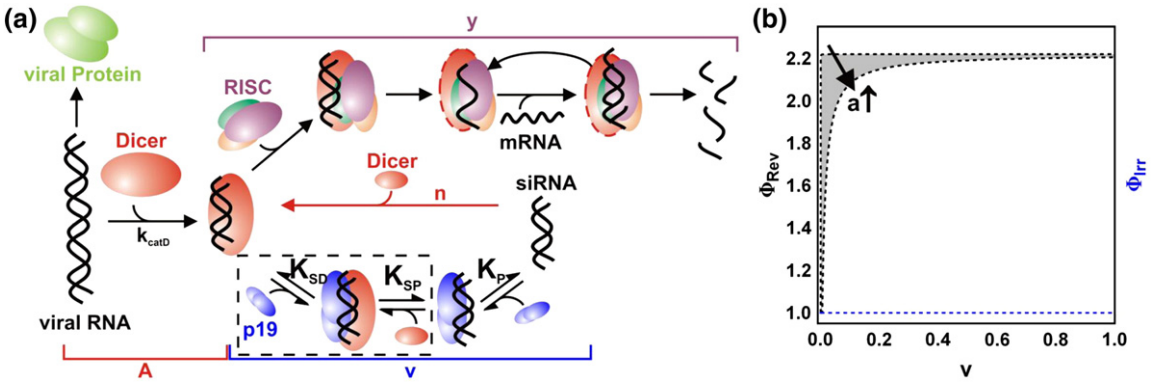

Fig. 5. Steady-state kinetic modeling of p19 action in RNAi suppression. (a) Schematic of our expanded "catch-and-release" mathematical model. *A*, *y*, and *v* describe the efficiencies of Dicer, RNAi in the cell, and p19, respectively. *n* is the fraction of siRNAs that successfully reenters the RNAi pathway after release from p19. The mature human RISC (with single-stranded siRNA bound) may or may not contain Dicer (dashed box). (b) Enhancement of viral protein load over unsuppressed protein level, assuming reversible and irreversible p19 binding (ϕ_{Rev} and ϕ_{Irr}, respectively). The fraction of SP complex over free p19 (*a*) will increase as the efficiency of p19 (*v*) increases. The enhancement in the level of viral protein due to reversible p19 binding will therefore fall within the range (gray area) determined for *a* ranging from 0.1 (upper bound) to 200 (lower bound).

dissociation equilibrium constant ($K_d = 0.37 \pm 0.08$ nM; Fig. 2) within 2.2-fold of the high affinity previously estimated from gel-based, inherently non-equilibrium EMSAs.[15] The dissociation of siRNA from p19 is nearly 3 orders of magnitude faster than that observed for many high-affinity nucleic acid–protein complexes, with dissociation rate constants on the order of 10^{-4} s^{-1}.[24,25,44,45] Strikingly, the rate and equilibrium constants for the SP complex resemble those of the human immunodeficiency virus-1 protein Rev for interaction with the Rev response element RNA ($k_{on} = 5.3 \times 10^8$ M^{-1} s^{-1}; $k_{off} = 0.14$ s^{-1}), perhaps due to the similarly (primarily) non-sequence-specific binding of a small protein to a (partially) base-paired RNA duplex.[46]

The presence of even low concentrations of p19 dramatically weakens the interaction of recombinant human Dicer with its siRNA product (25-fold to >270-fold, depending on the p19 concentration; Fig. 3a) in the absence of other detectable RISC components. Conversely, the presence of saturating concentrations of Dicer only slightly lowers (~4-fold) the affinity of p19 for siRNA (Fig. 3b), supporting the hypothesis that strong competition with the SD complex is an important mode of p19 action *in vivo*. Accordingly, assembly assays show that p19 also strongly disrupts the RISC-related human siRNA–protein complexes observed in HeLa cell extract that we show to contain all core RISC-loading complex components (Dicer, Ago2, and TRBP;[5] Fig. S1d and e), suggesting that p19 is able to disrupt the SD complex even in the context of the full complement of RISC components (Fig. 4). Our experimental results inform the mathematical modeling of the competition between Dicer and p19 for siRNA, as well as of the steady-state interactions between siRNA, Dicer, p19, RISC, and viral (m)RNA. We determine that the minimal model necessary to achieve the experimentally observed level of competition of p19 with Dicer for siRNA

Table 1. Model parameters

Name	Description (units)	Determined from	Value
k_{cat_D}	Catalytic rate of Dicer (nM h^{-1})	Ma *et al.*[34]	8.143×10^6
r_{dp}	Protein degradation rate constant (h^{-1})	Bartlett and Davis[35]	0.35
r_{ds}	siRNA degradation rate constant (h^{-1})	Bartlett and Davis[35]	0.029
k_{off}	p19 dissociation rate constant (h^{-1})	Determined experimentally	223.2
k_{on}	p19 association rate constant (nM^{-1} h^{-1})	Determined experimentally	608.4
N	Fraction of siRNA that reenters the RNAi pathway	Rose *et al.*[36]	0.01
A	Fraction of bound *versus* unbound p19	Estimated from experimental data	1–100
Cellular volume	Intracellular volume (l)	Bartlett and Davis[35]	1.4×10^{-12}
Grouped parameters			
y	RNAi efficacy parameter specific for HEK293 cells	Marshall[33]	1.22
A	Dicer efficacy parameter	k_{cat_D}/r_{dp}	2.33×10^7
β	RNAi settling time	r_{ds}/r_{dp}[33]	8.29×10^{-2}
v	p19 efficacy parameter	Range	0–1

requires the postulation of a transient ternary complex that favors dissociation into the SP complex and free Dicer (Fig. 3). In addition, an expanded steady-state kinetic model predicts a significant enhancement in viral protein load when the SP interaction is assumed to be reversible, as observed experimentally. Our results thus invoke a multiple-turnover "catch-and-release" mechanism wherein p19, unlike the released siRNA,[6,37] is effectively recycled after successfully competing with Dicer (Fig. 5). Notably, if the dissociation rate constant of the SP complex were lower and thus closer to that of a slow-release protein, p19 would be more efficient in competing with Dicer for siRNA but also less efficient in releasing the siRNA to achieve multiple turnover. It is tempting to speculate that evolution in this way has yielded a p19 with siRNA binding properties optimized for RNAi suppression.

As any mathematical model, our model relies on some assumptions, including an experimentally derived estimate for a low probability n of 1% for the reincorporation of siRNA released from p19 into the RNAi pathway.[6,37] The dependence of the predicted RNAi suppression has a relatively shallow dependence on n and, for any $n<1$, predicts an enhancement of suppression through the experimentally observed reversibility of the SP interaction. Strikingly, the estimated 2.2-fold enhancement in RNAi suppression through reversible SP complex formation is similar in magnitude to the typical RNAi effect that microRNAs (miRNAs) have on the expression of cellular genes,[9,47] suggesting that even a modest change in gene expression level as predicted here can have profound biological consequences, in our case on the likelihood of the survival of a virus in its host.

Several implications for the struggle between the virus and the cellular RNAi machinery arise from our work. First, in gene therapeutic applications, p19 will be required to be effective outside of its natural host environment, where a study of the protein's potential interaction partners so far has been lacking. Here, we observe p19 in the context of human cellular components and find evidence for ternary complex formation between p19, an siRNA, and human Dicer. Our experimental data suggest that the observed efficient competition of p19 with the SD complex (Fig. 3) and with the resulting Dicer-containing RISC assembly complexes (Fig. 4) targets a particularly critical step on the path to an activated RISC. Recent three-dimensional reconstructions from negatively stained electron microscopy images of human Dicer complexes depict it as a fist-like shape with a central flat surface that is thought to bind the siRNA.[4,48,49] This architecture, along with the known binding mode of p19, raises the possibility that p19 could bind the opposite face of the siRNA in a ternary complex with Dicer. Notably, crystal structures of several other viral suppressors also appear to bind only one face of the siRNA, leaving the opposite face open to potentially accommodate proteins such as Dicer.[50] While we did not observe the formation of a supershifted band as indicative of such a ternary complex in our EMSAs with siRNA, p19, and human Dicer (Fig. 4d–g), the complex may simply be too short-lived or our EMSA may simply be too low in resolution for the complex to be detected.

Second, the previously proposed simple sequestration model would require stoichiometric p19 concentrations relative to all siRNA duplexes (native to CIRV or not) generated by Dicer, as well as all other small duplex RNAs bound by p19, including defective interfering RNAs,[20] siRNA amplification products generated in plant and other cells by RNA-dependent RNA polymerase activity,[2,51] and perhaps miRNA duplexes.[19,52,53] We independently confirmed the ability of p19 to bind a human miRNA using the conserved, ubiquitous, and well-studied let-7a miRNA, which has been implicated as a tumor suppressant.[54] Remarkably, we observed that p19 binds the partially mismatched, double-stranded 22-nucleotide let-7a miRNA and our 21-nucleotide siRNA with equal affinities of 0.16 ± 0.02 nM and 0.17 ± 0.03 nM, respectively (Fig. S8). Similar to our observations, a recent study used an affinity-capture approach to show that p19 from CIRV retains a high affinity for let-7 miRNA, as well as a fluorophore-labeled siRNA.[53] These observations further underscore that p19 may face a large background of competitor RNAs while targeting its siRNA substrate, although the specific base-pairing patterns of some plant miRNAs may disfavor their binding to p19.[55] Our finding that formation of the high-affinity SP complex is readily reversible (Fig. 2) while still interfering with siRNA binding by Dicer and RISC-related assembly complexes *in vitro* (Figs. 3 and 4) raises the possibility that substoichiometric p19 concentrations may suffice *in vivo* to prevent siRNAs (by multiple turnover) from assembling into RISC. In this fashion, the virus could keep pace with the amplified host response during systemic RNAi self-defense of the plant host against CIRV.[56]

Third, while our results have an immediate impact on our understanding of the physicochemical properties and biological function of p19, a more practical consideration also arises from our work. The future of RNAi-based strategies may well be dependent on the ability to control and predict the relative intracellular expression levels of RISC components and potential therapeutics.[40,57] For example, short hairpin RNAs, while shown *in vivo* to efficiently induce gene silencing, have been found in long-term investigations to cause dose-dependent liver injury and ultimately death in adult mice when sustained at high levels,[57] and to cause dysregulation of miRNAs and increased tumorigenesis when

marginally dosed.[58] Coexpression with p19 could help ameliorate such toxic effects of short hairpin RNAs. In addition, CIRV p19 and other RSS have been shown to aid in the transfection and difficult overexpression of alpha viruses, adenoviruses, and lentiviruses used in gene therapy and plant-based vaccines, through their ability to suppress the intracellular RNAi immune response.[40] For such immunosuppression to be effective, dosing of the RSS is important, analogous to the use of immunosuppressants after organ transplant surgery. In fact, our observation that at least some miRNAs tightly bind to p19 cautions that adverse developmental effects due to a sequestration of essential cellular RNAs have to be carefully avoided. Understanding and modeling relevant biophysical properties of RNAi processes in the presence of RSS, as advanced here, are thus anticipated to become critical for a broader and safer use of RNAi therapeutics in human disease control.

Materials and Methods

Sources of p19, Dicer, HeLa cell extract, and RNA

Purified p19 protein was prepared as previously described,[15] and its dimer concentration was measured by Bradford assay. Recombinant human Dicer was prepared by Genlantis using the Baculovirus system with a commercially available protocol from Invitrogen. The His-tagged Dicer was purified on a Ni^{2+} column, and the His tag was removed by Tev protease cleavage, which should remove any contaminating factors that do not remain bound to the recombinant Dicer. S100 cytosolic HeLa cell extract was obtained from Jena Biosciences, and the integrity of Dicer in both samples was tested by Western blot analysis (Fig. S1a). Additionally, we demonstrated the biological activity of the recombinant Dicer through cleavage assays using long double-stranded RNA substrates (Fig. S1b). An estimate of Dicer concentration in the partially purified preparation was derived from Bradford assays to measure the total protein concentration in combination with the 5% purity quoted by Genlantis and verified by Coomassie staining of a denaturing SDS-PAGE gel (Fig. S1c). This estimate is conservative, as higher relative purities would only imply that even higher concentrations of Dicer are needed to efficiently compete with p19 for siRNA binding. All RNAs were synthesized by the HHMI Biopolymer/Keck Foundation Biotechnology Resource Laboratory at the Yale University School of Medicine, then deprotected and purified as previously described.[27,59] siRNA sequences were derived from the firefly luciferase gene,[26] as follows: sense strand 5′-P-CGU ACG CGG AAU ACU UCG AAA-3′ and antisense strand 5′-P-UCG AAG (fluorescein-dT)AU UCC GCG (amino C6-dT)AC GUG-3′, where P denotes a 5′-phosphate, and fluorescein-dT and amino C6-dT denote the phosphoramidites of the same name from Glen Research; the antisense strand was also synthesized with only one or no modification wherein U replaced the modified dT. Where needed, tetramethylrhodamine was coupled to the amino C6 linker, and the RNA was purified as described previously.[59] miRNA sequences were derived from the human wild-type let-7a miRNA, as follows: let-7a antisense strand 5′-P-UGA GGU AGU AGG UUG UAU AGU U-3′ and let-7a sense strand 5′-P-CUA UAC AAU CUA CUG UCU UUC C-3′.

Steady-state fluorescence spectroscopy

Standard fluorescence measurements were performed on an Aminco Bowman spectrofluorometer (Thermo Scientific) at 37 °C. siRNA duplexes were formed by mixing an excess of 100 nM unlabeled sense strand with 50 nM labeled sense strand in near-physiologic standard buffer [50 mM Tris-acetate (pH 7.4), 80 mM KCl, 20 mM NaCl, 1 mM $MgCl_2$, 1 mM DTT, and 0.02% (vol/vol) Tween 20], heat annealing for 2 min at 70 °C, and cooling to room temperature over 5 min. T/F doubly labeled siRNAs were excited at 490 nm (4 nm slit width), and emission was alternately detected at 520 nm (for fluorescein) and 585 nm (8 nm slit width for tetramethylrhodamine) to calculate the T/F ratio; fluorescein or tetramethylrhodamine singly labeled siRNAs were excited/detected at 490 nm/520 nm or 565 nm/585 nm, respectively. In a typical experiment, p19 was added to 50 nM labeled siRNA and mixed manually to a final concentration of 500 nM, unless otherwise indicated. For a chase experiment, unmodified siRNA duplex (formed by annealing the unlabeled composite sense and antisense RNA strands in a 2:1 ratio in standard buffer) was added to a final concentration of 3 μM. Saturation by the chase was ensured by triplicate trials using 500 nM, 750 nM, 1.5 μM, and 3 μM (Fig. S2).

To observe fast SP complex formation, we prepared siRNA samples as described above in standard buffer to a final concentration of 40 nM. In standard buffer, p19 was added to varying (at least 8-fold) final excess concentrations (0.32–1.76 μM) at 37 °C in a KinTek PMA23B stopped-flow spectrofluorometer while exciting at 520 nm and detecting emission at 585 nm. All time courses were fitted with single-exponential increase or decrease functions in Origin (OriginLab) as described previously.[60]

Electrophoretic mobility shift assays

For radioactive EMSAs, the nonphosphorylated antisense strand was first 5′-^{32}P-labeled with T4 polynucleotide kinase and [γ-^{32}P]ATP at an RNA concentration of 800 nM. Polynucleotide kinase was inactivated by heating to 90 °C for 10 min, then the 5′ phosphorylated complementary strand was added in 2-fold molar excess, and the reaction was slowly cooled to room temperature to anneal the two strands. The siRNA duplex was further purified by nondenaturing 20% (wt/vol) PAGE. The duplex siRNA was cut out, eluted overnight into 1 mM ethylenediaminetetraacetic acid (EDTA) at 4 °C, ethanol precipitated, and dissolved in RNase-free water. Scintillation counting was performed on a Beckman LS6500 Multipurpose Scintillation Counter. EMSAs were performed[15] on 10-cm nondenaturing 12% (wt/vol) polyacrylamide gels in 0.5× TBE (44.5 mM Tris-borate and 1 mM EDTA) and run at 500 V and 4 °C for 2 h, as described previously. Dicer and p19 at varying final concentrations were added to radiolabeled

siRNA duplex (50,000 cpm, <400 pM 5′-^{32}P-labeled duplex) in 10 μl of standard buffer and incubated for 0.5 h. Next, 10 μl of nondenaturing loading buffer (10% glycerol, 0.5× TBE, 0.025% bromophenol blue, and 0.025% xylene cyanol) was added, and each sample was loaded into a well of the EMSA gel. Competition experiments were performed by preincubating <400 pM siRNA duplex (prepared as described above) in standard buffer either with 140 nM Dicer and increasing concentrations of p19, or with 0.17 nM or 2.5 nM p19 and increasing concentrations of Dicer. Gel-chase experiments were performed in standard buffer with 70 nM and 10 nM Dicer or p19, respectively, to <400 pM 5′-^{32}P-labeled siRNA and with addition of 750 nM unlabeled siRNA chase for 0 min, 10 min, 30 min, 60 min, and 120 min. Gels were wrapped in plastic wrap and exposed to phosphor screens, which were scanned on a Storm 840 PhosphorImager and quantified using Image Quant software (Molecular Dynamics). The relative fraction f of relevant protein complexes was fitted with the following hyperbolic binding isotherm to extract the saturation point f_{max} and the half-titration point $K_{d,app}$:

$$f = f_{max}\frac{[\text{protein}]}{[\text{protein}] + K_{d,app}}$$

RISC assembly complex formation

To observe RISC assembly complexes, we incubated 15%, 50%, or 75% (vol/vol) cytosolic HeLa cell extract with <400 pM siRNA duplex (prepared as described above) in a final volume of 10 μl of HeLa buffer—8% (vol/vol) lysis buffer [23.7 mM Hepes (pH 7.5), 79 mM potassium acetate, 1.58 mM magnesium acetate, 5 mM DTT, and 1 mg ml^{-1} Perabloc SC (Roche)], supplemented with 20% (vol/vol) 5× RNAi mix (125 mM creatine phosphate, 5 mM ATP, and 25 mM DTT), 2% (wt/vol) creatine kinase, and 20% (vol/vol) RNA guard RNase Inhibitor (GE Bioscience)—for 2 h at 4 °C, unless otherwise specified. For competition experiments, p19 was added in increasing concentrations to the HeLa cell extract/siRNA mixture either immediately or after a 2-h preincubation. Time courses were stopped by direct loading onto a running nondenaturing 4% (wt/vol) polyacrylamide gel in 0.5× TBE, then run at ~50 mW cm^{-2} and 4 °C. For comparison with a previous assay, 50% and 75% (vol/vol) HeLa cell extract was incubated with siRNA as described by Pellino *et al.* for 1 h at 4–37 °C and analyzed by EMSA, yielding similar results (Fig. S4).[28] Fifteen percent (vol/vol) extract was preferred for most of our work due to the better pH control afforded by this lower concentration and to conserve material. For antibody supershift EMSA, cytosolic HeLa cell extract (24 μg of total protein) was preincubated with 0.8 μg or 1.6 μg of anti-Dicer rabbit polyclonal antibody (Santa Cruz Biotechnology, Inc.) and 0.8 μg or 1.6 μg of unrelated control antibodies—either anti-DsRed rabbit polyclonal antibody (Clontech Laboratories, Inc.) or anti-β actin mouse monoclonal antibody (Sigma-Aldrich, Inc.)—for 2 h at 4 °C prior to the RISC assembly assay. The final volume was 60 μl per lane. Nondenaturing 4% (wt/vol) PAGE was used to resolve these complexes, as described above. Time courses and titration curves were fitted as described above.

Time-resolved FRET

Time-resolved donor (fluorescein) fluorescence decays were collected in the presence and in the absence of acceptor (tetramethylrhodamine) using time-correlated single-photon counting, as previously described.[61,62] As before, the donor decay in the presence of acceptor was modeled as a weighted average of the decays for each donor–acceptor distance in the ensemble of molecules assuming a three-dimensional Gaussian distance distribution with a Förster distance of 54 Å between fluorescein and tetramethylrhodamine.[61,62]

Western blot analyses for Dicer detection

For denaturing Western blot analyses, the cytosolic HeLa cell extract, the recombinant Dicer enzyme preparation, and the recombinant TRBP (Abcam) and Ago2 (Abnova) proteins were run on a NuPAGE Novex 4–12% gradient 2-[bis(2-hydroxyethyl)amino]-2-(hydroxymethyl)propane-1,3-diol gel in the presence of a molecular weight marker (ECL Plex Rainbow marker). The gel was then electroblotted in Tris-glycine buffer [25 mM Tris, 192 mM glycine, and 20% (vol/vol) methanol] onto a polyvinylidene fluoride membrane (Immobilon-P Membrane; Millipore) over 75 min at 300 mA, using a Bio-Rad Trans-Blot SD semidry transfer cell as per the manufacturer's instructions. After transfer, the membrane was probed with rabbit anti-Dicer antibody (Santa Cruz Biotechnology) and mouse anti-TRBP or mouse anti-Ago2 antibody (both Abnova), followed by goat anti-rabbit-Cy5 and goat anti-mouse-Cy3 antibodies (both Amersham), respectively. The probed blots in Fig. S1a, d, and e were visualized on a Typhoon 9410 Variable Mode Imager (GE Healthcare Life Sciences).

For nondenaturing Westerns blot analyses, RISC assembly complexes were formed as described above, but reactions were scaled up by 6-fold. Gels were soaked in 0.1% (wt/vol) SDS for 15 min and then electroblotted in Tris-glycine transfer buffer (25 mM Tris and 25 mM glycine) onto a polyvinylidene fluoride membrane (Immobilon-P Membrane; Millipore) over 75 min at 300 mA, using a Bio-Rad Trans-Blot SD semidry transfer cell as per the manufacturer's instructions. After transfer, the proteins were fixed to the membrane by incubating in 5–10% (vol/vol) acetic acid, rinsing with deionized water, and air drying. The membrane was probed with a rabbit primary antibody against Dicer (Santa Cruz Biotechnology), followed by a goat anti-rabbit secondary antibody conjugated with horseradish peroxidase (Zymed; Invitrogen). The blot was developed using a peroxide/enhancer solution (ECL-Plus detection; Amersham) and visualized on a Typhoon 9410 Variable Mode Imager (Fig. S5).

Modeling p19 in the context of RNAi

For the model described schematically in (Fig. 5a), changes in viral protein expression levels were monitored at steady state in the absence and in the presence of the RSS p19. Changes in free p19 protein over time depend on terms representing the natural rates of production ($r_x r_t / r_{dm}$), degradation (r_{dp} [p19]), extent of siRNA binding (k_{on} [siRNA] [P]), and SP complex dissociation (k_{off} [SP]).

Production of p19 is governed by its transcription rate (r_x), its messenger RNA (mRNA) degradation rate (r_{dm}), and its translation rate (r_t), which are assumed to have reached equilibrium on a timescale faster than that of repression. The p19 protein is degraded by the first-order rate constant (r_{dp}), leading to:

$$\text{p19}'[\tau] = \frac{r_x r_t}{r_{dm}} - r_{dp}[\text{p19}] - k_{on}[\text{siRNA}][\text{p19}] + k_{off}[\text{SP}] \quad (1)$$

The amount of usable siRNA in the system (i.e., the fraction that is able to associate with RISC) is reduced by the amount of siRNA bound to p19. Production of siRNA is dependent on the catalytic rate constant of Dicer (k_{cat_D}), and siRNA is degraded with a first-order rate constant (r_{ds}). The parameter n is the fraction of siRNA that reenters the RNAi pathway after p19 dissociation, yielding:

$$\text{siRNA}'[\tau] = k_{cat_D}[\text{Dicer}] - r_{ds}[\text{siRNA}] - k_{on}[\text{siRNA}][\text{p19}] + nk_{off}[\text{SP}] \quad (2)$$

The time evolution of the viral protein of interest that serves as a reporter of RNAi suppression and p19 enhancement is described as:

$$\text{viral}'[\tau] = \frac{r_x r_t}{\frac{k_{cat_R}}{K_{DR}}[\text{RISC}][\text{siRNA}] + r_{dm}} - r_{dp}[viral] \quad (3)$$

where (k_{cat_R}) is the catalytic rate constant for the RISC-mediated cleavage of mRNA. The additional term in the denominator of Eq. (3) is a quasi-steady-state assumption used in previous work[33,63] to describe RISC-mediated degradation of viral mRNA. It assumes that the active concentration of siRNA-loaded RISC approaches its steady-state value with the rate constant k_{cat_R}. This buildup of siRNA-loaded RISC contributes to the rate of degradation of the viral mRNA, as described by the concentrations of RISC and siRNA, as well as the dissociation constant K_{dr}. The proteins not silenced by RNAi are represented at steady state by unitless constants:

$$[\text{Dicer}] = \frac{r_x r_t}{r_{dp} r_{dm}} \quad (4)$$

$$[\text{RISC}] = \frac{r_x r_t}{r_{dp} r_{dm}} \quad (5)$$

Equations (1)–(3) are rescaled as described by Marshall and solved at steady state to yield:[33]

$$P = \frac{1}{1 - Aa\frac{k_{off}}{k_{cat_D}} + (Av\beta)S} \quad (6)$$

$$S = \frac{1 + \frac{k_{off}}{k_{cat_D}} naP}{\beta + \beta v P} \quad (7)$$

$$V = \frac{1}{1 + \beta y S} \quad (8)$$

where y and β are the parameters previously described as the efficiency of the RNAi pathway and the RNAi settling time, respectively.[33] The parameters a, v, and A are the fraction of siRNA-bound p19 relative to total p19, the efficiency of p19, and the efficiency of Dicer in a particular cell line, respectively. The level of the viral protein at steady state is dependent mostly on S. For example, in the absence of RNAi (i.e., in the absence of Dicer), $S=0$, so that $V=1$ (i.e., the viral protein level is not suppressed). Substituting Eq. (6) into Eq. (7) yields two solutions for S, where we choose S_2 as the more biologically relevant one:

$$S_1 = \frac{1 - aA\frac{k_{off}}{k_{cat_D}} + v - Av + \sqrt{\left(-4A\left(-1 + a\frac{k_{off}}{k_{cat_D}}(A - n)\right)\frac{v}{\beta^2} + \left(-1 + aA\frac{k_{off}}{k_{cat_D}} + (-1 + A)v\right)^2\right)}}{2Av\beta}$$

$$S_2 = \frac{1 - aA\frac{k_{off}}{k_{cat_D}} + v - Av - \sqrt{\left(-4A\left(-1 + a\frac{k_{off}}{k_{cat_D}}(A - n)\right)\frac{v}{\beta^2} + \left(-1 + aA\frac{k_{off}}{k_{cat_D}} + (-1 + A)v\right)^2\right)}}{2Av\beta} \quad (9)$$

Substituting S_2 into Eq. (8) yields:

$$V_{Rev} = \frac{1}{1 + \frac{y\left(1 - aA\frac{k_{off}}{k_{cat_D}} + v - Av - \sqrt{\left(-4A\left(-1 + a\frac{k_{off}}{k_{cat_D}}(A - n)\right)\frac{n}{\beta^2} + \left(-1 + aA\frac{k_{off}}{k_{cat_D}} + (-1 + A)v\right)^2\right)}\right)}{2Av}} \quad (10)$$

If p19 binding is assumed to be irreversible (i.e., $k_{off}=0$), then V solves to:

$$V_{Irr} = \frac{2Av}{\left(-1 - v + \sqrt{1 + 2(1 + A)v + (-1 + A)^2 v^2}\right)y + Av(2 + y)} \quad (11)$$

In the absence of p19 (i.e., $P=0$), based on Eqs. (7) and (8), V reduces to the fully suppressed protein level:

$$V_o = \frac{1}{1+y} \tag{12}$$

The enhancement of viral protein production due to either irreversible (ϕ_{Irr}) or reversible (ϕ_{Rev}) p19 binding is then found to be (see also Fig. 5b):

$$\phi_{Irr} = \frac{V_{Irr}}{V_o} \tag{13}$$

$$\phi_{Rev} = \frac{V_{Rev}}{V_o} \tag{14}$$

Supplementary materials related to this article can be found online at doi:10.1016/j.jmb.2011.02.038

Acknowledgements

We thank Jeffrey Vargason and Traci Hall for the generous provision of purified p19 protein, as well as Patrick Nelson for helpful discussions on mathematical modeling. We also thank Jennifer Doudna for providing analytical quantities of purified Dicer and Ago protein. This work was funded by National Institutes of Health grant GM081025 (N.G.W.) and a National Academy of Science Ford fellowship (R.A.R.).

References

1. Fire, A., Xu, S., Montgomery, M. K., Kostas, S. A., Driver, S. E. & Mello, C. C. (1998). Potent and specific genetic interference by double-stranded RNA in *Caenorhabditis elegans*. *Nature*, **391**, 806–881.
2. Carthew, R. W. & Sontheimer, E. J. (2009). Origins and mechanisms of miRNAs and siRNAs. *Cell*, **136**, 642–655.
3. Castanotto, D. & Rossi, J. J. (2009). The promises and pitfalls of RNA-interference-based therapeutics. *Nature*, **457**, 426–433.
4. Sashital, D. G. & Doudna, J. A. (2010). Structural insights into RNA interference. *Curr. Opin. Struct. Biol.* **20**, 90–97.
5. MacRae, I. J., Ma, E., Zhou, M., Robinson, C. V. & Doudna, J. A. (2008). *In vitro* reconstitution of the human RISC-loading complex. *Proc. Natl Acad. Sci. USA*, **105**, 512–517.
6. Kim, D. H., Behlke, M. A., Rose, S. D., Chang, M. S., Choi, S. & Rossi, J. J. (2005). Synthetic dsRNA Dicer substrates enhance RNAi potency and efficacy. *Nat. Biotechnol.* **23**, 222–226.
7. Collingwood, M. A., Rose, S. D., Huang, L., Hillier, C., Amarzguioui, M., Wiiger, M. T. *et al.* (2008). Chemical modification patterns compatible with high potency Dicer–substrate small interfering RNAs. *Oligonucleotides*, **18**, 187–200.
8. Ji, X. (2008). The mechanism of RNase III action: how Dicer dices. *Curr. Top. Microbiol. Immunol.* **320**, 99–116.
9. Siomi, H. & Siomi, M. C. (2009). On the road to reading the RNA-interference code. *Nature*, **457**, 396–404.
10. Jaskiewicz, L. & Filipowicz, W. (2008). Role of Dicer in posttranscriptional RNA silencing. *Curr. Top. Microbiol. Immunol.* **320**, 77–97.
11. Gitlin, L. & Andino, R. (2003). Nucleic acid-based immune system: the antiviral potential of mammalian RNA silencing. *J. Virol.* **77**, 7159–7165.
12. Parameswaran, P., Sklan, E., Wilkins, C., Burgon, T., Samuel, M. A., Lu, R. *et al.* (2010). Six RNA viruses and forty-one hosts: viral small RNAs and modulation of small RNA repertoires in vertebrate and invertebrate systems. *PLoS Pathog.* **6**, e1000764.
13. Qu, F. & Morris, T. J. (2005). Suppressors of RNA silencing encoded by plant viruses and their role in viral infections. *FEBS Lett.* **579**, 5958–5964.
14. Scholthof, H. B. (2006). The Tombusvirus-encoded p19: from irrelevance to elegance. *Nat. Rev. Microbiol.* **4**, 405–411.
15. Vargason, J. M., Szittya, G., Burgyan, J. & Hall, T. M. (2003). Size selective recognition of siRNA by an RNA silencing suppressor. *Cell*, **115**, 799–811.
16. Ye, K., Malinina, L. & Patel, D. J. (2003). Recognition of siRNA by a viral suppressor of RNA silencing. *Nature*, **426**, 874–878.
17. Xia, Z., Zhu, Z., Zhu, J. & Zhou, R. (2009). Recognition mechanism of siRNA by viral p19 suppressor of RNA silencing: a molecular dynamics study. *Biophys. J.* **96**, 1761–1769.
18. Lakatos, L., Szittya, G., Silhavy, D. & Burgyan, J. (2004). Molecular mechanism of RNA silencing suppression mediated by p19 protein of tombusviruses. *EMBO J.* **23**, 876–884.
19. Dunoyer, P., Lecellier, C. H., Parizotto, E. A., Himber, C. & Voinnet, O. (2004). Probing the microRNA and small interfering RNA pathways with virus-encoded suppressors of RNA silencing. *Plant Cell*, **16**, 1235–1250.
20. Havelda, Z., Hornyik, C., Valoczi, A. & Burgyan, J. (2005). Defective interfering RNA hinders the activity of a tombusvirus-encoded posttranscriptional gene silencing suppressor. *J. Virol.* **79**, 450–457.
21. Omarov, R., Sparks, K., Smith, L., Zindovic, J. & Scholthof, H. B. (2006). Biological relevance of a stable biochemical interaction between the tombusvirus-encoded p19 and short interfering RNAs. *J. Virol.* **80**, 3000–3008.
22. Lakatos, L., Csorba, T., Pantaleo, V., Chapman, E. J., Carrington, J. C., Liu, Y. P. *et al.* (2006). Small RNA binding is a common strategy to suppress RNA silencing by several viral suppressors. *EMBO J.* **25**, 2768–2780.
23. Merai, Z., Kerenyi, Z., Kertesz, S., Magna, M., Lakatos, L. & Silhavy, D. (2006). Double-stranded RNA binding may be a general plant RNA viral strategy to suppress RNA silencing. *J. Virol.* **80**, 5747–5756.
24. Mitsis, P. G. & Wensink, P. C. (1989). Identification of yolk protein factor 1, a sequence-specific DNA-

binding protein from *Drosophila melanogaster*. *J. Biol. Chem.* **264**, 5188–5194.
25. Ramsden, J. J. & Dreier, J. (1996). Kinetics of the interaction between DNA and the type IC restriction enzyme EcoR124II. *Biochemistry*, **35**, 3746–3753.
26. Martinez, J., Patkaniowska, A., Urlaub, H., Luhrmann, R. & Tuschl, T. (2002). Single-stranded antisense siRNAs guide target RNA cleavage in RNAi. *Cell*, **110**, 563–574.
27. Hoerter, J. A. & Walter, N. G. (2007). Chemical modification resolves the asymmetry of siRNA strand degradation in human blood serum. *RNA*, **13**, 1887–1893.
28. Pellino, J. L., Jaskiewicz, L., Filipowicz, W. & Sontheimer, E. J. (2005). ATP modulates siRNA interactions with an endogenous human Dicer complex. *RNA*, **11**, 1719–1724.
29. Pham, J. W. & Sontheimer, E. J. (2005). Separation of *Drosophila* RNA silencing complexes by native gel electrophoresis. *Methods Mol. Biol.* **309**, 11–16.
30. Pham, J. W., Pellino, J. L., Lee, Y. S., Carthew, R. W. & Sontheimer, E. J. (2004). A Dicer-2-dependent 80S complex cleaves targeted mRNAs during RNAi in *Drosophila*. *Cell*, **117**, 83–94.
31. Sigurskjold, B. W. (2000). Exact analysis of competition ligand binding by displacement isothermal titration calorimetry. *Anal. Biochem.* **277**, 260–266.
32. Wreggett, K. A. & De Lean, A. (1984). The ternary complex model. Its properties and application to ligand interactions with the D2-dopamine receptor of the anterior pituitary gland. *Mol. Pharmacol.* **26**, 214–227.
33. Marshall, W. F. (2008). Modeling recursive RNA interference. *PLoS Comput. Biol.* **4**, e1000183.
34. Ma, E., MacRae, I. J., Kirsch, J. F. & Doudna, J. A. (2008). Autoinhibition of human Dicer by its internal helicase domain. *J. Mol. Biol.* **380**, 237–243.
35. Bartlett, D. W. & Davis, M. E. (2006). Insights into the kinetics of siRNA-mediated gene silencing from live-cell and live-animal bioluminescent imaging. *Nucleic Acids Res.* **34**, 322–333.
36. Rose, S. D., Kim, D. H., Amarzguioui, M., Heidel, J. D., Collingwood, M. A., Davis, M. E. *et al.* (2005). Functional polarity is introduced by Dicer processing of short substrate RNAs. *Nucleic Acids Res.* **33**, 4140–4156.
37. Hefner, E., Clark, K., Whitman, C., Behlke, M. A., Rose, S. D., Peek, A. S. *et al.* (2008). Increased potency and longevity of gene silencing using validated Dicer substrates. *J. Biomol. Tech.* **19**, 231–237.
38. Chu, M., Desvoyes, B., Turina, M., Noad, R. & Scholthof, H. B. (2000). Genetic dissection of tomato bushy stunt virus p19-protein mediated host-dependent symptom induction and systemic invasion. *Virology*, **266**, 79–87.
39. Silhavy, D., Molnar, A., Lucioli, A., Szittya, G., Hornyik, C., Tavazza, M. *et al.* (2002). A viral protein suppresses RNA silencing and binds silencing-generated, 21- to 25-nucleotide double-stranded RNAs. *EMBO J.* **21**, 3070–3080.
40. de Vries, W., Haasnoot, J., van der Velden, J., van Montfort, T., Zorgdrager, F., Paxton, W. *et al.* (2008). Increased virus replication in mammalian cells by blocking intracellular innate defense responses. *Gene Ther.* **15**, 545–552.
41. Lombardi, R., Circelli, P., Villani, M. E., Buriani, G., Nardi, L., Coppola, V. *et al.* (2009). High-level HIV-1 Nef transient expression in *Nicotiana benthamiana* using the p19 gene silencing suppressor protein of Artichoke Mottled Crinckle Virus. *BMC Biotechnol.* **9**, 96.
42. Zheng, N., Xia, R., Yang, C., Yin, B., Li, Y., Duan, C. *et al.* (2009). Boosted expression of the SARS-CoV nucleocapsid protein in tobacco and its immunogenicity in mice. *Vaccine*, **27**, 5001–5007.
43. Qian, S., Zhong, X., Yu, L., Ding, B., de Haan, P. & Boris-Lawrie, K. (2009). HIV-1 Tat RNA silencing suppressor activity is conserved across kingdoms and counteracts translational repression of HIV-1. *Proc. Natl Acad. Sci. USA*, **106**, 605–610.
44. Mougel, M., Ehresmann, B. & Ehresmann, C. (1986). Binding of *Escherichia coli* ribosomal protein S8 to 16S rRNA: kinetic and thermodynamic characterization. *Biochemistry*, **25**, 2756–2765.
45. Seimiya, M. & Kurosawa, Y. (1996). Kinetics of binding of Antp homeodomain to DNA analyzed by measurements of surface plasmon resonance. *FEBS Lett.* **398**, 279–284.
46. Pond, S. J., Ridgeway, W. K., Robertson, R., Wang, J. & Millar, D. P. (2009). HIV-1 Rev protein assembles on viral RNA one molecule at a time. *Proc. Natl Acad. Sci. USA*, **106**, 1404–1408.
47. Krol, J., Loedige, I. & Filipowicz, W. (2010). The widespread regulation of microRNA biogenesis, function and decay. *Nat. Rev. Genet.* **11**, 597–610.
48. Lau, P. W., Potter, C. S., Carragher, B. & MacRae, I. J. (2009). Structure of the human Dicer–TRBP complex by electron microscopy. *Structure*, **17**, 1326–1332.
49. Wang, H. W., Noland, C., Siridechadilok, B., Taylor, D. W., Ma, E., Felderer, K. *et al.* (2009). Structural insights into RNA processing by the human RISC-loading complex. *Nat. Struct. Mol. Biol.* **16**, 1148–1153.
50. Yang, J. & Yuan, Y. A. (2009). A structural perspective of the protein–RNA interactions involved in virus-induced RNA silencing and its suppression. *Biochim. Biophys. Acta*, **1789**, 642–652.
51. Lipardi, C. & Paterson, B. M. (2009). Identification of an RNA-dependent RNA polymerase in *Drosophila* involved in RNAi and transposon suppression. *Proc. Natl Acad. Sci. USA*, **106**, 15645–15650.
52. Chapman, E. J., Prokhnevsky, A. I., Gopinath, K., Dolja, V. V. & Carrington, J. C. (2004). Viral RNA silencing suppressors inhibit the microRNA pathway at an intermediate step. *Genes Dev.* **18**, 1179–1186.
53. Jin, J., Cid, M., Poole, C. B. & McReynolds, L. A. (2010). Protein mediated miRNA detection and siRNA enrichment using p19. *Biotechniques*, **48**, xvii–xxiii.
54. Boyerinas, B., Park, S. M., Hau, A., Murmann, A. E. & Peter, M. E. (2011). The role of let-7 in cell differentiation and cancer. *Endocr.-Relat. Cancer*, **17**, F19–F36.
55. Varallyay, E., Valoczi, A., Agyi, A., Burgyan, J. & Havelda, Z. (2010). Plant virus-mediated induction of miR168 is associated with repression of ARGONAUTE1 accumulation. *EMBO J.* **29**, 3507–3519.
56. Baulcombe, D. (2004). RNA silencing in plants. *Nature*, **431**, 356–363.

57. Grimm, D., Streetz, K. L., Jopling, C. L., Storm, T. A., Pandey, K., Davis, C. R. *et al.* (2006). Fatality in mice due to oversaturation of cellular microRNA/short hairpin RNA pathways. *Nature*, **441**, 537–541.
58. Beer, S., Bellovin, D. I., Lee, J. S., Komatsubara, K., Wang, L. S., Koh, H. *et al.* (2010). Low-level shRNA cytotoxicity can contribute to MYC-induced hepatocellular carcinoma in adult mice. *Mol. Ther.* **18**, 161–170.
59. Walter, N. G. (2002). Probing RNA structural dynamics and function by fluorescence resonance energy transfer (FRET). *Curr. Protoc. Nucleic Acid Chem.* 11.10.11–11.10.23.
60. Gondert, M. E., Tinsley, R. A., Rueda, D. & Walter, N. G. (2006). The catalytic core structure of the trans-acting HDV ribozyme is subtly influenced by sequence variation outside the core. *Biochemistry*, **45**, 7563–7573.
61. Rueda, D., Wick, K., McDowell, S. E. & Walter, N. G. (2003). Diffusely bound Mg^{2+} ions slightly reorient stems I and II of the hammerhead ribozyme to increase the probability of formation of the catalytic core. *Biochemistry*, **42**, 9924–9936.
62. Gerczei, T., Shah, B. N., Manzo, A. J., Walter, N. G. & Correll, C. C. (2009). RNA chaperones stimulate formation and yield of the U3 snoRNA–pre-rRNA duplexes needed for eukaryotic ribosome biogenesis. *J. Mol. Biol.* **390**, 991–1006.
63. Groenenboom, M. A., Maree, A. F. & Hogeweg, P. (2005). The RNA silencing pathway: the bits and pieces that matter. *PLoS Comput. Biol.* **1**, 155–165.